

# P-type Cu<sub>7</sub>Te<sub>5</sub> single-crystalline nanocuboids: size-controlled synthesis and large-scale self-assembly†

 Cite this: *CrystEngComm*, 2014, 16, 9441

 Received 31st March 2014,  
Accepted 13th May 2014

Baosong Dai, Qian Zhao, Jing Gui, Jiatao Zhang\* and Hesun Zhu

DOI: 10.1039/c4ce00670d

[www.rsc.org/crystengcomm](http://www.rsc.org/crystengcomm)

Cu<sub>7</sub>Te<sub>5</sub> single-crystalline nanocuboids have been synthesized by a low-temperature solvothermal strategy, using environmentally friendly chemicals. The size, from nanometer to sub-micrometer, was controlled by adjusting the dodecanethiol (DDT) concentration. Through DDT capping, which induced appropriate van der Waals interactions, the alignment of the nanocuboids led to large-scale self-assembly of superstructures or supracrystals. The UV-vis-NIR spectra of the as-prepared nanocuboid colloid exhibited potential LSPR properties. Measurement of the Mott–Schottky impedance potential curve confirmed the p-type conductivity of the as-prepared Cu<sub>7</sub>Te<sub>5</sub> nanocuboids.

## 1. Introduction

Copper telluride (Cu<sub>2-x</sub>Te) nanocrystals (NCs) have composition-, size- and shape-dependent properties, such as near-infrared (NIR) localized surface plasmon resonance (LSPR), thermoelectric and ionic conductivity properties, which enable their potential application in surface-enhanced Raman scattering (SERS), photothermal conversion, solar cells, and electroconductive electrodes.<sup>1–3</sup> They are usually p-type semiconductors because of the presence of copper vacancies. Copper vacancies not only determine the charge transport properties, but also provide composition-dependent LSPR properties.<sup>4,5</sup> By adjusting the Cu:Te ratio, copper tellurides (Cu<sub>2-x</sub>Te) can exist in a wide range of compositions and phases. Thus, well-defined composition, shape and uniform size control are important in controlling the LSPR and transport properties. Many groups, such as the Tuan, Cabot, Feldmann, and Yu groups, have studied the synthesis and properties of copper telluride nanostructures.<sup>3–7</sup> However, a facile strategy for more flexible size control of Cu<sub>2-x</sub>Te NCs,

from nanometer to micrometer, is still required in order to control their optical and electronic properties. There are few reports on the synthesis and properties of Rickardite Cu<sub>7</sub>Te<sub>5</sub> NCs.<sup>3–12</sup> In this paper, without the addition of special precursors, we use the environmentally friendly common chemicals, copper stearate, trioctylphosphine telluride (TOP-Te) and oleic acid (OA) in toluene solvent to synthesize Cu<sub>7</sub>Te<sub>5</sub> nanocuboids with flexible size control using a low-temperature solvothermal method.

Monodisperse NCs can self-assemble into superstructures under the appropriate conditions of temperature, solvent and coating agents.<sup>13</sup> These self-assemblies can exhibit tunable physical and chemical properties, but also lay the foundation for assembly-based optoelectronic nanodevices. The self-assembly of nanocubes by dipole–dipole interactions which enables face-to-face alignment has been researched by the Yang, Xia, and Fang groups, among others.<sup>11–16</sup> Research on the self-assembly of nanocuboids has only obtained limited progress because of their flexible anisotropic rectangular shapes.<sup>17</sup> In particular, not only the shape and size of the NCs, but also the uniform nanogaps between the NCs, can distinctly affect LSPR properties. Here, by this new synthesis strategy, good monodispersity, large-scale monolayers, multi-layer self-assembly and different assembling modes of Cu<sub>7</sub>Te<sub>5</sub> nanocuboids have been realized. Confirmation of the p-type conductivity and the LSPR properties of the Cu<sub>7</sub>Te<sub>5</sub> nanocuboids have also been investigated.

## 2. Experimental section

### 2.1 Copper stearate (CuSt<sub>2</sub>) preparation

All chemicals were used without further processing. CuSt<sub>2</sub> was synthesized according to the literature.<sup>18</sup> Typically, 2.5 mmol (0.4262 g) CuCl<sub>2</sub>·2H<sub>2</sub>O and 5 mmol (1.5323 g) of sodium stearate were dissolved in a mixture of 10 mL distilled water, 70 mL hexane and 50 mL methanol at 60 °C for 4 h. The upper organic layer containing CuSt<sub>2</sub> was

Research Center of Materials Science, School of Materials Science & Engineering, Beijing Institute of Technology, Beijing 100081, PR China. E-mail: zhangjt@bit.edu.cn; Fax: +86 1068918065; Tel: +86 10 68918065

† Electronic supplementary information (ESI) available: Fig. S1–S3 and the analysis of the largest exposed faces of the crystal. See DOI: 10.1039/c4ce00670d

decanted and washed several times.  $\text{CuSt}_2$  in solid form was finally obtained after total evaporation of the residual hexane and methanol.

## 2.2 Top-Te organic precursor preparation

1 mmol (0.128 g) Te powder was dissolved in 3 mmol (1.34 mL) TOP at 150 °C under nitrogen for more than 2 h, until the Te powder was completely dissolved. Then we obtained a clear yellow solution which was diluted in toluene solvent.

## 2.3 Synthesis of $\text{Cu}_7\text{Te}_5$ nanocuboids

Typically, 0.25 mmol  $\text{CuSt}_2$  was dissolved in 5 mL toluene to obtain a clear solution, then 6 mL oleic acid (OA) was introduced into the solution and 2 mL of the Top-Te precursor was added. After this was stirred for 5 min, 2 mL dodecanethiol (DDT) was introduced to get a homogeneous solution. Then, it was transferred into a Teflon-lined autoclave with 25 mL capacity. The autoclave was sealed and heated at 150 °C for 1 h. The product was washed with 20 mL of methanol several times.

## 2.4 Characterization

Samples for characterization by TEM and electron diffraction were prepared by adding one drop of toluene colloid containing the product onto a 300 mesh nickel grid with carbon support film. Low resolution transmission electron microscopy (LRTEM), carried out by a JEOL JEM-1200EX instrument working at 100 kV, and high-resolution transmission electron microscopy (HRTEM), carried out by a FEI Tecnai G2 F20 S-Twin instrument working at 200 kV, were utilized to characterize the morphology, monodispersity, self-assembly and crystallization details. SEM images and energy-dispersive spectrometry (EDS) analysis were obtained from the sample on a silicon substrate, using a Hitachi FE-SEM 4800 instrument. Samples for XRD measurements were prepared by adding several drops of concentrated product onto silicon (100) wafers and drying at room temperature. The phases of the products were determined by XRD on a Bruker D8 Advance X-ray power diffractometer with  $\text{CuK}\alpha$  radiation ( $\lambda = 1.5418 \text{ \AA}$ ). The ultraviolet-visible-near-infrared (UV-vis-NIR) absorption spectra of the  $\text{Cu}_7\text{Te}_5$  nanocuboid toluene colloids were recorded on a Shimadzu UV3600 UV-vis-NIR spectrophotometer at room temperature. Confirmation of the p-type conductivity of the  $\text{Cu}_7\text{Te}_5$  nanocuboids was carried out by measurement of the Mott-Schottky impedance potential curves. These were measured on an IM6e electrochemical workstation (Zahner, Germany) with a standard three-electrode system, namely, the working electrode, the Pt counter electrode, and the  $\text{Ag}/\text{AgCl}$  reference electrode. As-prepared  $\text{Cu}_7\text{Te}_5$  nanocuboid film (which underwent vacuum drying treatment at 100 °C for 3 h) on indium tin oxide (ITO) glass was used as the working electrode. The electrolyte was a 200 ml solution of 0.1 M NaOH and 0.1 M  $\text{Na}_2\text{S}$ .

## 3. Results and discussion

As illustrated by the LRTEM images in Fig. 1A and S1,<sup>†</sup> monodisperse nanocuboids with a size of 5.9 nm were prepared with high purity. The HRTEM image in Fig. 1B confirmed the single-crystallinity of the nanocuboids. Based on indexing, the distance measured between two adjacent fringes were 0.70 nm and 0.50 nm, which should be assigned to the (002) plane (0.61 nm) and (032) plane (0.45 nm) of Rickardite  $\text{Cu}_7\text{Te}_5$  (JCPDS #26-1117). The corresponding fast Fourier transform (FFT) pattern (inset of Fig. 1B) contains diffraction spots from the (032) and (030) planes of the orthorhombic phase  $\text{Cu}_7\text{Te}_5$ , and belongs to [100].<sup>19</sup> In other words, the largest exposed faces of the crystal belong to highly-indexed [100] planes.<sup>20</sup> By adjusting the concentration of DDT ligand, flexible size control was realized. As shown in Fig. 1C and D, the LRTEM and HRTEM images exhibited single-crystalline nanocuboids with a size of about 10–12 nm. The indexed lattice spacings and the inserted electron diffraction pattern in Fig. 1D are consistent with Fig. 1B. Fig. 1E shows nanocuboids with a size of about 100 nm, and Fig. 1F shows the sub-micrometer size produced without DDT addition. With increasing size, the size range becomes bigger, and the rectangular shape becomes more anisotropic, which finally produces micrometer-sized nanoplate shapes. The rhombus shaped nanoplates with large size range in Fig. 1F are reasonable because of the orthorhombic crystal phase. The powder XRD pattern of the nanocuboids in Fig. 2A also confirms the Rickardite phase (JCPDS # 26-1117). The EDS pattern from large-scale SEM analysis of the samples on a silicon substrate in Fig. 2B exhibits a Cu : Te ratio of about 1.5, which is concordant with the  $\text{Cu}_7\text{Te}_5$  phase confirmed by the XRD and ED characterizations. The strong Si signal comes from the silicon substrate.

The advantage of our synthesis method is not only the flexible size control, but also the realization of self-assembly of the as-prepared nanocuboids on a large scale. In this work, we found that when the size of the as-prepared  $\text{Cu}_7\text{Te}_5$  nanocuboids was ~5.9 nm, they were more similar to nanocubes and the monodispersity was good. As illustrated by the size analysis shown in Fig. 3A, more than 94% of the nanocuboids are in the range of 5.8–6.0 nm. Due to the good monodispersity of nanocuboids, and DDT capping, which can provide appropriate van der Waals interactions between the nanocrystals,<sup>21–26</sup> the large-scale self-assembly of nanocuboids is realized easily, as shown in Fig. 3A, B and S2.<sup>†</sup> Here, DDT is an important factor to get large-scale self-assembly. Fig. 3A exhibits the monolayer self-assembly. The FFT pattern of the multi-layer self-assembly (inset in Fig. 3B) confirmed that the face-to-face simple-cubic close packing formed a superlattice. As studied by the Xia, Yang and Fang groups,<sup>14–17</sup> the dipole-dipole interactions promoted face-face alignments. This kind of multi-layer superlattice can be expanded on a bulk film scale, as shown in the digital photo in the inset of Fig. 3B. This large-scale assembly of the nanocuboid film has potential for photothermal and photovoltaic device applications.<sup>27,28</sup> The superstructure formed by the

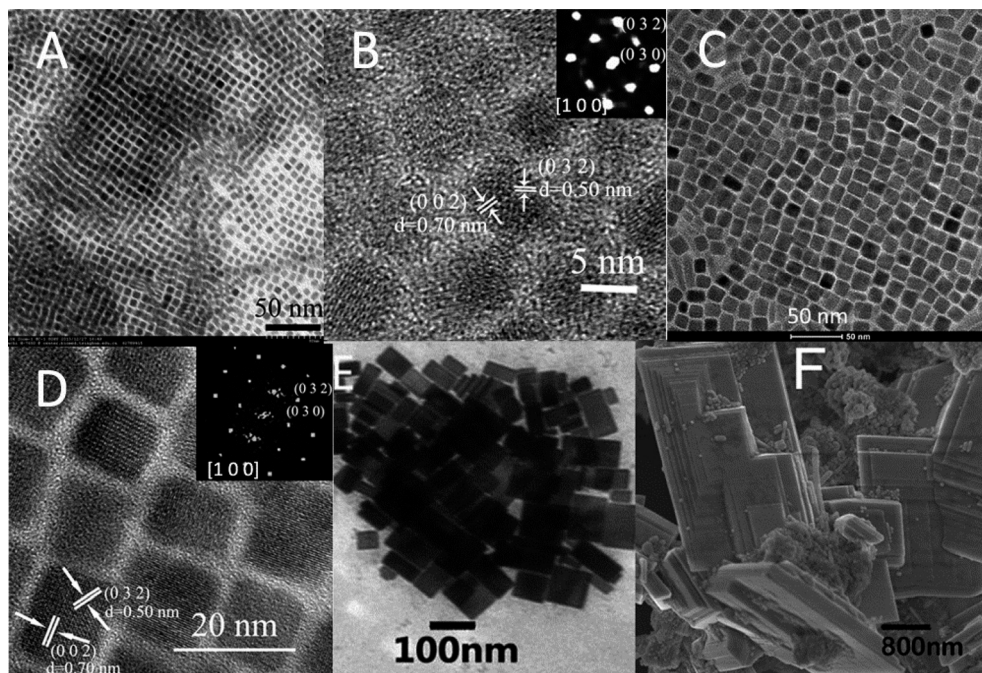


Fig. 1 LRTEM and HRTEM morphologies (A–E) and SEM morphology (F) of  $\text{Cu}_7\text{Te}_5$  nanocuboids, from nanometer size to sub-micrometer size. The FFT pattern and ED pattern are shown in the insets of Fig. B and D.

hierarchical assembly of the nanocuboids was further characterized by scanning TEM (STEM), as shown in Fig. 3C. Through DDT capping, which enabled three-dimensional

ordered alignment of the nanocuboids, the micrometer-sized superstructures could form (see Fig. S3†). As with the shape evolution shown in Fig. 1, when the size becomes bigger, the anisotropic shape of the nanocuboid becomes more and more distinct. Without good monodispersity, the nanocuboids in Fig. 1C and E have no long-range-ordered self-assembly. However, the micrometer-sized nanoplates in Fig. 1D assemble face-to-face into superstructures on a large scale, as shown in Fig. 3D.

The LSPR properties of the  $\text{Cu}_{2-x}\text{Te}$  nanocrystals in the NIR region could be utilised in a broad range of applications, from optoelectronics and photothermal therapy to biomedicine.<sup>1–4,27,28</sup> Fig. 4A shows the UV-vis-NIR spectra of colloidal  $\text{Cu}_7\text{Te}_5$  nanocuboids with two sizes. A strong absorption band centered at 900–1000 nm is clearly observed. This is attributed to the LSPR of the nanocuboids. It was already confirmed that the nanocube shape had a stronger LSPR than the nanoplate and nanorod shaped nanocrystals in the NIR region.<sup>4</sup> Therefore, the as-prepared monodisperse  $\text{Cu}_7\text{Te}_5$  nanocuboids, which are similar to nanocubes, and their self-assembly, have the potential for use in surface enhanced Raman scattering (SERS) detection and photothermal therapy.

P-type  $\text{Cu}_{2-x}\text{Te}$  nanocrystals, due to copper vacancy determined efficient charge transport, can potentially be used for p/n heterojunction solar cell applications. According to the Mott–Schottky equation, for a p-type semiconductor,<sup>29,30</sup>

$$\frac{1}{C_{sc}^2} = -\frac{2}{\epsilon_0 \epsilon_r N_A A^2} \left( E - E_{FB} - \frac{kT}{e} \right) \quad (1)$$

where  $C_{sc}$  is the space charge region capacitance,  $\epsilon_0$  and  $\epsilon_r$  are the vacuum and relative dielectric permittivities,  $A$  is the

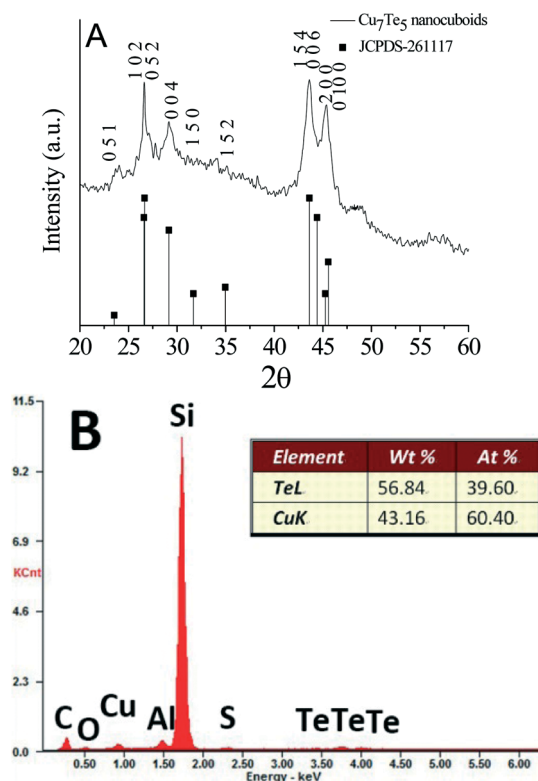
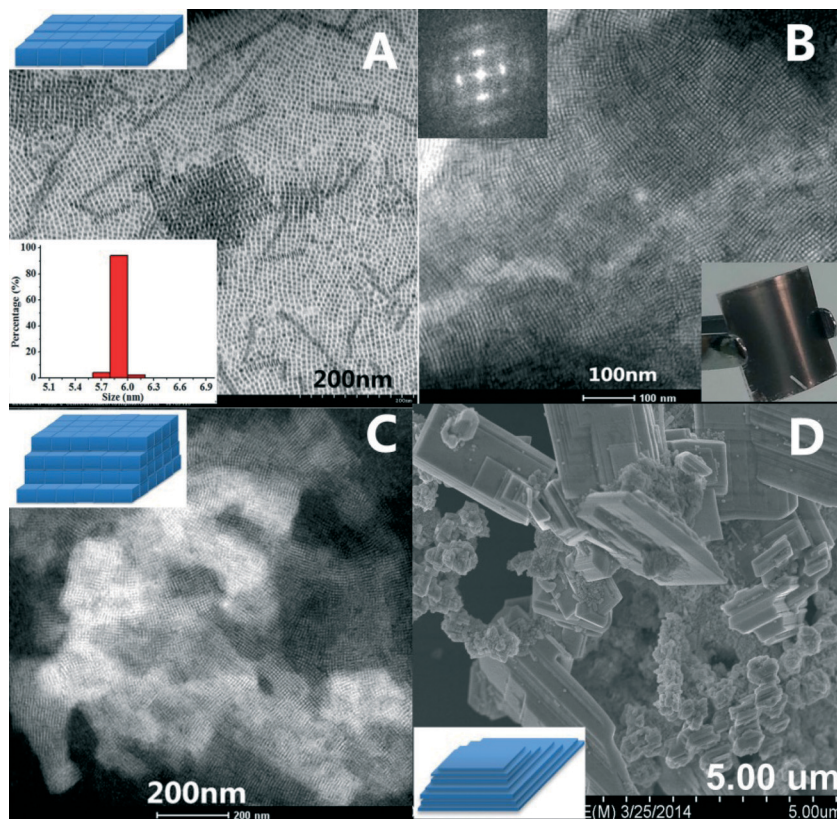
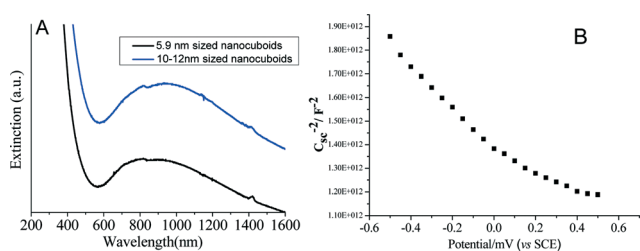


Fig. 2 A) XRD pattern of the as-prepared  $\text{Cu}_7\text{Te}_5$  nanocuboids. The pattern for bulk Rickardite  $\text{Cu}_7\text{Te}_5$  (JCPDS # 26-1117) is provided for reference and comparison. B) EDS pattern and Cu : Te ratio by SEM analysis.



**Fig. 3** HRTEM and STEM images of the monolayer self-assembly (A), large-scale multi-layer superlattice (B, C), and large-scale hierarchical assembly of  $\text{Cu}_7\text{Te}_5$  nanocuboids into superstructures (D). The size analysis for the  $\sim 5.9$  nm nanocuboids is shown in the inset of Fig. A. The drawings in the insets of Fig. A, C and D are provided to highlight the face-to-face assembly. The FFT pattern of the assembly and a photograph of the bulk-sized film on the flexible substrate are shown in the insets of Fig. B.

surface area of the sample in the electrolyte,  $N_A$  is the concentrations of acceptors,  $k$  is the Boltzmann constant,  $T$  is the temperature,  $E$  is the potential, and  $E_{\text{FB}}$  is flat band potential. A typical Mott–Schottky plot for the  $\text{Cu}_7\text{Te}_5$  nanocuboid film ( $1/C_{\text{sc}}^2$  versus the applied potential, where  $C_{\text{sc}}$  is the space charge region capacitance) is shown in Fig. 4B, from which the n or p-type conductivity can be identified.<sup>30</sup> The negative slope of all of the linear parts confirmed the p-type conductivity of the as-prepared  $\text{Cu}_7\text{Te}_5$  nanocuboids. Based on the confirmation of the p-type conductivity, potential use in a p/n heterojunction solar cell and optoelectronic device applications could be carried out next.



**Fig. 4** A) UV-vis-NIR spectra of the as-prepared  $\text{Cu}_7\text{Te}_5$  nanocuboid colloid. B) Typical Mott–Schottky plot for the  $\text{Cu}_7\text{Te}_5$  nanocuboid film in 0.1 M  $\text{Na}_2\text{S}$  and 0.1 M  $\text{NaOH}$  at 1 kHz. The potentials are measured with respect to the standard calomel electrode (SCE).

## 4. Conclusion

In summary, we developed a low-temperature solvothermal method to synthesize single-crystalline  $\text{Cu}_7\text{Te}_5$  nanocuboids with flexible size control. Thanks to DDT capping and shape uniformity, dipole–dipole interactions promote large-scale self-assembly of the nanocuboids. The strong LSPR properties exhibited in the NIR region indicate the potential of as-prepared  $\text{Cu}_7\text{Te}_5$  nanocuboids in sensitive detection and photothermal therapy applications. Confirmation of the p-type conductivity suggests potential application in photovoltaic devices.

## Acknowledgements

This work was supported by the Natural Science Foundation of China (91123001, 21322105, and 51371015), funding support from the Ministry of Education, China (NCET-11-0793, 2011101120016), and the Program for Beijing Excellent Talents (no. 2012D009011000007).

## References

- 1 J. M. Luther, P. K. Jain, T. Ewers and A. P. Alivisatos, *Nat. Mater.*, 2011, **10**, 361–366.

- 2 Y. Zhao and C. Burda, *Energy Environ. Sci.*, 2012, 5, 5564–5576.
- 3 I. Kriegel, C. Jiang, J. Rodríguez-Fernández, R. D. Schaller, D. V. Talapin, E. da Como and J. Feldmann, *J. Am. Chem. Soc.*, 2012, 134, 1583–1590.
- 4 W. H. Li, R. Zamani, P. R. Gil, B. Pelaz, M. Ibáñez, D. Cadavid, A. Shavel, R. A. Alvaerz-Puebla, W. J. Parak, J. Arbiol and A. Cabot, *J. Am. Chem. Soc.*, 2013, 135, 7098–7101.
- 5 H. Yang, C. Chen, F. Yuan and H. Tuan, *J. Phys. Chem. C*, 2013, 117, 21955–21964.
- 6 I. Kriegel, J. Rodríguez-Fernández, A. Wisnet, H. Zhang, C. Waurisch, A. Eyhmüller, A. Dubavik, A. O. Govorov and J. Feldmann, *ACS Nano*, 2013, 7, 4367–4377.
- 7 J. Liu, J. Xu, H. Liang, K. Wang and S. Yu, *Angew. Chem., Int. Ed.*, 2012, 51, 7420–7425.
- 8 Q. Wang, G. Chen, D. Chen and R. Jin, *CrystEngComm*, 2012, 14, 6962–6973.
- 9 Y. Zhang, Y. Ni, X. Wang, J. Xia and J. Hong, *Cryst. Growth Des.*, 2011, 11, 4368–4377.
- 10 L. Zhang, Z. Ai, F. Jia, L. Liu, X. Hu and J. C. Yu, *Chem. – Eur. J.*, 2006, 12, 4185–4190.
- 11 H. Shen, X. Jiang, S. Wang, Y. Fu, C. Zhou and L. S. Li, *J. Mater. Chem.*, 2012, 22, 25050–25056.
- 12 H. B. Li, R. Brescia, M. Povia, M. Prato, G. Bertoni, L. Manna and I. Moreels, *J. Am. Chem. Soc.*, 2013, 135, 12270–12278.
- 13 M. P. Pileni, *J. Mater. Chem.*, 2011, 21, 16748–16758.
- 14 J. Henzie, M. Grünwald, A. Widmer-Cooper, P. L. Geissler and P. D. Yang, *Nat. Mater.*, 2012, 11, 131–137.
- 15 Z. Quan, H. W. Xu, C. Y. Wang, X. D. Wen, Y. X. Wang, J. L. Zhu, R. P. Li, C. J. Sheehan, Z. W. Wang, D. Smilgies, Z. P. Luo and J. Y. Fang, *J. Am. Chem. Soc.*, 2014, 136, 1352–1359.
- 16 M. Rycenga, J. M. McLellan and Y. N. Xia, *Adv. Mater.*, 2008, 20, 2416–2420.
- 17 Y. Nakagawa, H. Kageyama, Y. Oaki and H. Imai, *J. Am. Chem. Soc.*, 2014, 136, 3716–3719.
- 18 S. Li, H. Z. Wang, W. W. Xu, H. L. Si, X. J. Tao, S. Y. Lou, Z. L. Du and L. S. Li, *J. Colloid Interface Sci.*, 2009, 330, 483–487.
- 19 G. X. Hu, X. Cai and Y. H. Rong, *Fundamentals of Materials Science*, Shanghai Jiao Tong University Press Co., Ltd, China, 2th edn, 2006, pp. 19–35.
- 20 F. R. Zhou, P. L. Zhu, X. Z. Fu, R. Q. Chen, R. Sun and C. P. Wong, *CrystEngComm*, 2014, 16, 766–774.
- 21 Z. Zhuang, P. Qing, B. Zhang and Y. D. Li, *J. Am. Chem. Soc.*, 2008, 130, 10482–10484.
- 22 Q. Zhao, J. T. Zhang and H. S. Zhu, *Prog. Nat. Sci.: Mater. Int.*, 2013, 23, 588–592.
- 23 X. X. Xu and X. Wang, *J. Mater. Chem.*, 2009, 19, 3572–3575.
- 24 Z. Zhuang, Q. Peng, X. Wang and Y. D. Li, *Angew. Chem., Int. Ed.*, 2007, 46, 8174–8177.
- 25 E. V. Shevchenko, D. V. Talapin, N. A. Kotov, S. O'Brien and C. B. Murray, *Nature*, 2006, 40, 685–689.
- 26 Y. S. Xia, T. D. Nguyen, M. Yang, B. Lee, A. Santos, P. Podsiadlo, Z. Tang, S. C. Glotzer and N. A. Kotov, *Nat. Nanotechnol.*, 2011, 6, 580–585.
- 27 W. Lu, Q. Huang, C. Li and W. Chen, *Nanomedicine*, 2010, 5, 1161–1171.
- 28 C. Lin, W. Lee, M. Lu, S. Chen, M. Hung, T. Chan, H. Tsai, Y. Chueh and L. Chen, *J. Mater. Chem.*, 2012, 22, 7098–7100.
- 29 D. F. Underwood, T. Kippeny and S. J. Rosenthal, *J. Phys. Chem. B*, 2001, 105, 436–440.
- 30 A. Izgorodin, O. Winther, B. Winther and D. R. MacFarlane, *Phys. Chem. Chem. Phys.*, 2009, 11, 8532–8536.